

Capillarity-Based Reversible Super-Adhesion

Sarah Grice

Mechanical Engineering, University of Maryland, College Park

NNIN REU Site: Cornell NanoScale Science and Technology Facility, Cornell University, Ithaca, NY

NNIN REU Principal Investigator(s): Prof. Paul Steen, Chemical Engineering, Cornell University

NNIN REU Mentor(s): David Anderson, XiuMei Xu, Chemical Engineering, Cornell University

Contact: sgrice@umd.edu, phs7@cornell.edu, anderson.da@gmail.com, xx44@cornell.edu

Abstract:

This project draws inspiration from the palm beetle's defense mechanism by creating an adhesion pad in which a large array of water droplets is controlled by an electro-osmotic pump to achieve reversible super-adhesion. In order to enhance the adhesion performance, three modifications were made to a previous design. First, the droplet diameters were reduced from the previously fabricated 150-500 μm hole devices to 50-100 μm , which allows more liquid bridges per unit area and thereby increases the adhesion force. Second, a raised frame around the array was fabricated to allow easy detachment and is a first step in optimizing the liquid bridge length during attachment. Third, the depth of the water reservoir was varied. The functionality of these devices was tested.

Introduction / Background:

The palm beetle defends itself from predators by using small droplets of oil that it manipulates using the bristles of its tarsi. These droplets form liquid bridges with a substrate leaf, allowing the beetle to stick with a force equivalent to approximately 60-100 times its body weight. When the danger has passed, the beetle can then break these liquid bridges and continue on its way, leaving behind small amounts of oil residue.

This strategy is ideal for creating reversible adhesion, which has been accomplished by creating adhesion pads that use large arrays of droplets of water in place of the palm beetle's oil. Such devices are predicted to increase in the adhesive force per unit area they can exert as the droplet size is decreased. However, scaling features down in size is a significant fabrication challenge.

Objectives:

The goal of this project was to create a new generation of adhesion pads that would reduce the droplet diameter from 100 μm to 50 and 75 μm . Two variations on the basic design of the adhesion pad were also fabricated: first, a raised lip or frame around the array of holes was created on half the plates created, and second, the depth of the water reservoir was varied.

Device Design and Operation:

The adhesion pad consists of a sandwich of silicon plates with an array of holes fabricated in them using a reactive ion etcher (Labels 1 and 5 in Figure 1). These plates are coated on their inside-facing sides with a thin gold electrode (Labels 2

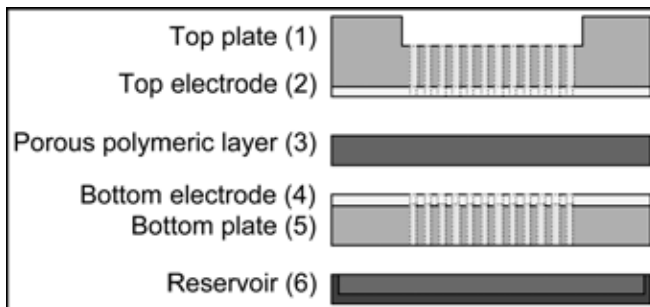


Figure 1: Adhesion pad design.

and 4). A porous polymeric layer—in the case of the devices fabricated, made of polyethersulfone, or PES—is placed between the plates (3), and a small reservoir of water (6) is attached to the bottom.

When a voltage is applied across the electrodes, electro-osmosis, enhanced by the small pores of the PES layer, pulls water up from the reservoir and forces it out of the holes in the top plate. This creates an ordered array of droplets, which may then contact a substrate and form liquid bridges.

Fabrication and Testing:

Three adhesion devices were assembled: (1) a 75 μm unframed device with a 6 mm deep reservoir, (2) a 50 μm framed device, and (3) a 75 μm unframed device with a 2 mm deep reservoir.

Two types of tests were performed on the devices: syringe-pumped tests and electro-osmosis-pumped tests. In the first

case, water was forced into the device's reservoir using a syringe and tube arrangement. In the second case, voltage was applied across the PES layer so that electro-osmosis could be used to move the water.

Results:

Syringe-Pumped Testing. Difficulties in assembly and testing made overall array uniformity difficult to achieve with syringe testing. Pump condition and position proved especially important to overall performance, as porous layer misalignment resulted in the formation of abnormally large droplets.

In comparing their performance during syringe pumping, the shallow (2 mm) and deep (6 mm) reservoir devices were shown to have roughly comparable droplet distributions after variations in assembly are discounted, as can be seen in Figures 2 and 3. This performance is surprising because the reservoir depth at which significant variation in droplet height from the edge to the center of the array was predicted to be around 2 mm.

Electro-Osmosis-Pumped Testing. Of the three devices tested, two of the electro-osmotic (EO) pumps were functional. In the case of the 50 μm framed device, EO pumping resulted in significantly better performance than syringe pumping, as holes or folds in the PES layer did not result in large droplets, as can be seen in Figure 4. EO pumping the 75 μm shallow reservoir device did not provide as much of an improvement in performance, and in fact seemed to increase the incidence of large droplet formation.

Conclusions and Future Work:

50 μm and 75 μm droplet diameter adhesion pads were fabricated, and initial tests of their functionality were carried out. These devices were found to have the best performance characteristics when operated using their integrated EO pump at relatively low voltages. The performance of shallow and deep reservoir devices during syringe pumping was found to be comparable after accounting for variations in assembly such as frit misalignment.

In the future, adhesion measurements of the assembled devices will be performed, determining how much adhesion force per unit area was gained relative to the reduction in droplet size.

Acknowledgements:

I would like to thank my wonderful PI, Prof. Paul Steen, and awesome mentors, David Anderson and Xiumei Xu, for all their support and encouragement during my time at Cornell. I would also like to acknowledge the National Nanotechnology Infrastructure Network Research Experience for Undergraduates Program and the National Science Foundation for helping to make this experience possible for me.

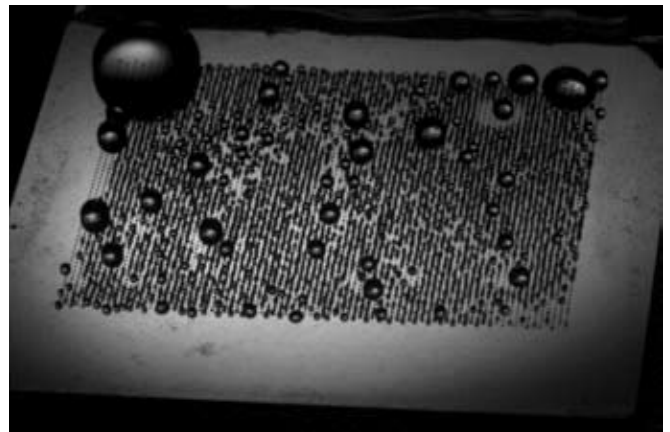
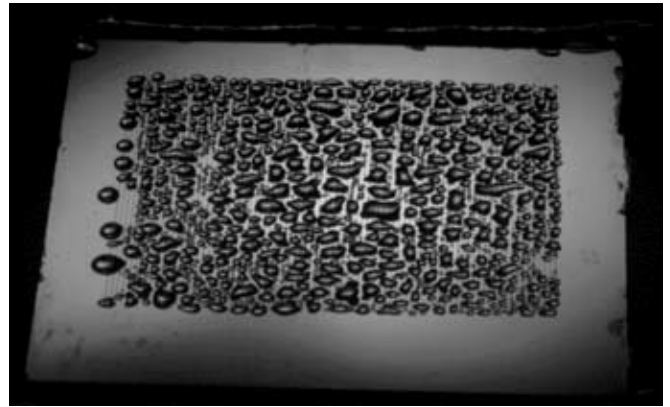


Figure 2, top: 75 μm shallow reservoir device, syringe pumped (photographed using a macro lens).

Figure 3, middle: 75 μm deep reservoir device, syringe pumped (photographed using a macro lens).

Figure 4, bottom: 50 μm deep reservoir device, EO pumped (photographed using a macro lens).

Fabrication of a Microelectromechanical Device for On-Chip Mechanical Testing of Nanoscale Thin Films in a Transmission Electron Microscope

Sarah Koehler

Mechanical Engineering, Cornell University

NNIN REU Site: Penn State Nanofabrication Facility, The Pennsylvania State University, State College, PA

NNIN REU Principal Investigator(s): Dr. Aman Haque, Mechanical and Nuclear Engr, The Pennsylvania State University

NNIN REU Mentor(s): Mohan Manoharan, Mechanical and Nuclear Engr, The Pennsylvania State University

Contact: smk269@cornell.edu, mah37@engr.psu.edu, mxm1002@psu.edu

Abstract:

Typically, deformation and failure mechanisms in materials and interfaces are studied either quantitatively (measuring stress-strain behavior) or qualitatively (post-mortem or off-line imaging with a microscope). The transmission electron microscope (TEM) is unique in the sense that it visualizes specimen microstructures (dislocations, grain boundaries, precipitates, cracks) with very high resolution. Therefore, if experiments could be conducted *in situ* inside a TEM, we could avoid ‘modeling’ as the tool for bridging the mutual exclusiveness of the quantitative and qualitative streams of materials behavior research. Unfortunately, the TEM chamber is very small; it allows a volume of 3 mm diameter and 0.5 mm thickness in which the specimen and the force and displacement sensors must be accommodated.

The objective of this research is to shrink an entire tensile testing machine (on the order of meters) to 3 mm diameter size using nanofabrication techniques. Such drastic miniaturization involves photolithography, thin film deposition and bulk micromachining techniques on both sides of a silicon-on-insulator (SOI) wafer.

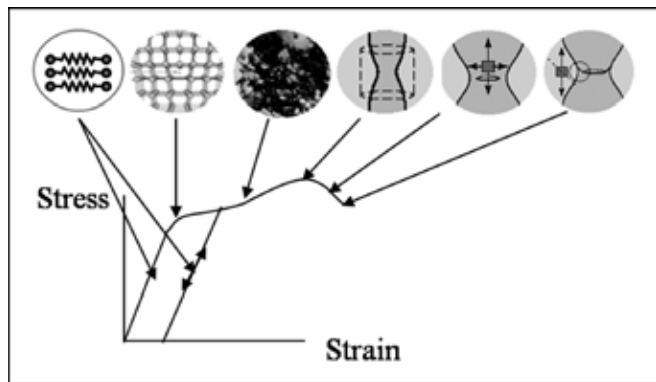


Figure 1: How materials fail—qualitatively and quantitatively.

Introduction:

Figure 1 includes a typical graph of stress versus strain that shows quantitative material deformation. The linear portion of the curve is the elastic region, where material deformation is reversible and the material acts much like an elastic spring. The non-linear portion of the curve is the plastic region, where deformations are irreversible, and dislocations have occurred in the material. The pictures above the graph demonstrate qualitative analysis of material deformation. We would like to be able to match up this qualitative and quantitative data better than we have previously been able to using post-mortem techniques.

The devices that we design for this purpose have to be capable of straining a nanoscale thin film while in the TEM. The design utilizes a thermal actuator to place a tensile load on the specimen. The thermal actuator consists of pairs of micro-beams, as seen in the right hand side of Figure 2. To actuate, a voltage is applied across the ends of the inclined beams actuator. This causes the beams to heat and expand. The beams are inclined so that the net force on the specimen (once the beams expand) is to the right in Figure 2.

Another important feature of the device is that it has a hole etched through the backside. This is needed because the TEM passes electrons through a specimen in order to acquire an

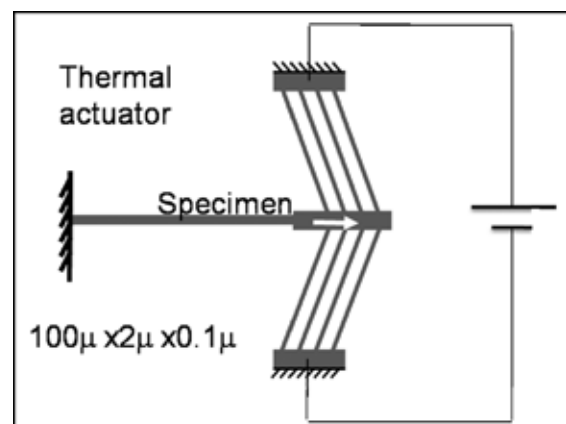


Figure 2: Diagram of thermal actuator.

image. The thick silicon layer is “opaque” to electrons, so it is important to have a nanoscale thin film that is free-standing above the backside hole.

Experimental Procedure:

The procedure for fabricating the devices consists of multiple lithography and etching steps. The devices were made on a silicon-on-insulator (SOI) wafer. The wafer consists of a 35 μm silicon device layer, a 1-2 μm silicon dioxide layer, and a 350 μm silicon handle layer. Before lithography processes begin, a metal layer on the order of nanometers was deposited on top of the device layer.

First, a 100 nm metal layer was evaporated onto the front side of the wafer. Next, the front side of the device was patterned using the Karl Suss MA 6/BA 6 lithography tool. The metal was then etched, and the silicon device layer was etched using deep reactive ion etching (DRIE). After these steps, the device was essentially complete except for the backside hole that is required for imaging in the TEM.

To etch the backside hole, a circular-shaped hole was patterned on to a thick photoresist (SPR 220-7) using the backside alignment technique in the Karl Suss MA 6/BA 6. DRIE was used again for anisotropic backside etching. The oxide was then etched anisotropically using the Plasma Therm. DRIE was again used to etch the device layer just underneath the specimen so that it would be freestanding. Finally, HF vapor was used to release the beams for mobility.

Results and Conclusions:

We were able to etch the frontside of several devices, but had more difficulty fabricating the backside hole. We were able to produce SEM compatible devices to nearly one hundred percent yield, but the backside hole required for TEM compatibility was more difficult to fabricate. The backside etching was a problem because the wafer broke easily during backside DRIE. The residual stress of the SOI wafer was a big factor contributing towards the breakage.

We were able to etch through the handle layer using a xenon difluoride (XeF_2) isotropic etch of silicon, and we completed the first backside etching of the device. Figure 4 shows the backside of a device that was successfully etched and we can see through the optically transparent silicon dioxide layer to the beams on the front side that attach the device to the SOI wafer.

Future Work:

We plan to continue developing a better method to etch the backside hole of the device. We will continue to etch isotropically with xenon difluoride, and may try a different mask with a smaller backside hole so that an isotropic etch is anticipated. Once the devices are successfully made, we will then do simultaneous quantitative and qualitative testing in the TEM.

Acknowledgements:

I would like to thank my principal investigator Aman Haque, my mentor Mohan Manoharan, and other members of our research group. Also, thanks to members of the Pennsylvania State University Nanofabrication Staff. I would also like to thank the National Nanotechnology Infrastructure Network Research Experience for Undergraduates Program and the National Science Foundation for funding.

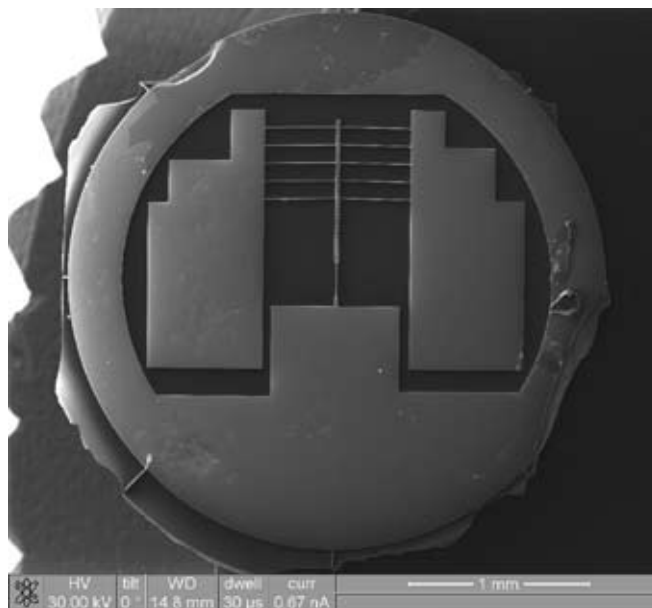


Figure 3: SEM image of a device.

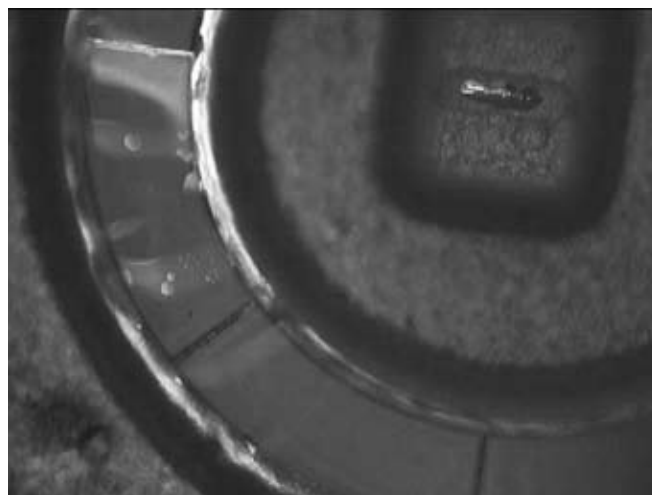


Figure 4: Backside image of a device with isotropically etched handle layer.

Optimization of MEMS Fabrication for Electrical Detection

Joshua Ott

Electrical Engineering, Southern Methodist University



**NNIN REU Site: Cornell NanoScale Science and Technology Facility,
Cornell University, Ithaca, NY**

NNIN REU Principal Investigator(s): Harold Craighead, Applied and Engineering Physics, Cornell University

NNIN REU Mentor(s): Darren Southworth, Josh Cross, Applied and Engineering Physics, Cornell University

Contact: hgc1@cornell.edu, drs59@cornell.edu, jdc47@cornell.edu

Abstract:

The much-celebrated potential of resonate microelectromechanical systems (MEMS) in sensing and electrical filter technologies has been limited by convenient methods of device readout. Our purpose is to optimize MEMS devices for electrical detection, enabling integration into real-world devices. We fabricated device arrays in which the parameters of etch orifice size, sacrificial oxide thickness, and device geometry were varied in order to maximize electrical coupling.

Introduction:

MEMS resonant technology is used for biological sensing and electric filtering technologies. These resonators have a certain resonance frequency. Shifts in resonant frequency from accretion of mass onto the device, for example, could indicate the presence of an analyte. We are developing an electrical method of resonance frequency detection. Historically, these resonators lack convenient methods of device readout. Some methods require large apparatus' such as superconducting magnets or aligned optics. With the advent of electrical detection we have a means for real-world integration of these devices since the simple circuitry required lends itself to packaging. All that is required is a capacitor and inductor.

In the past, electrical readout was limited by small signal detection. We fabricated device arrays with varied resonator geometries in attempt to increase the signal. The goal of these geometries was to reduce the motional resistance, which is the figure of merit in our experiment.

$$R_m = \frac{d^2 m \omega_0}{V_g^2 C_g^2 Q}$$

Figure 1: Motional resistance equation.

The motional resistance equation can be seen in Figure 1. Variable d is the sacrificial oxide thickness, m is the resonator mass, ω_0 is the angular frequency, V_g is the voltage applied to the resonators, C_g is the resonator capacitance, and Q is the quality factor.

We attempted to reduce motional resistance by changing the resonator geometries and etch hole orifices, which altered the variables m , ω_0 , and C_g . We also grew varying oxide thicknesses, which reduced the distance (d) and increased the capacitance (C_g). The resulting correlations gave the oxide

thickness a fourfold effect on the motional resistance, making it one of the most important aspects of our devices. However, if we created a thickness too thin, the devices would not resonate properly and stick to the silicon wafer.

Experimental Procedure:

An array of devices, including different geometries and different etch hole sizes, were fabricated on each die. The etch holes were created using a reactive ion etch. A buffered oxide etch was then used to release the resonators from the oxide.

The most important devices from fabrication were our "drums," a flat membrane with a single etch hole. This device can be seen in Figure 2. The light areas correspond to where the device is released from the wafer. The drums were created with etch hole diameter's varying from 2-10 μm , in 2 μm increments. Actual membrane diameters measured

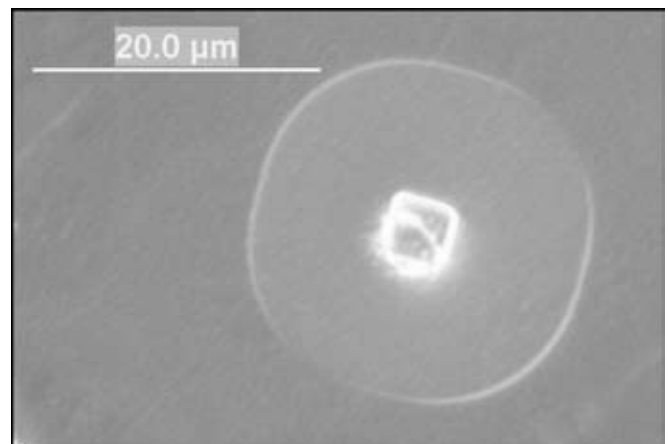


Figure 2: 4 μm etch hole drum resonator.

approximately 20 μm . The drums were comprised of polysilicon grown on silicon dioxide. The polysilicon was N⁺ doped, made tensile (in order to create a flat membrane) and grown to approximately 330 nm. Oxide thicknesses of 645, 223, and 95 nm were the targets, with 223 nm being the only viable resonator.

An LC impedance matching circuit was used to detect the electrical signal. The resonators were placed under vacuum. By interchanging capacitors and inductors, the circuit was matched to the resonance frequency of each resonator. Using LabView, the quality factor and resonance frequency was then calculated. With these variables we did back calculations to get the motional resistance.

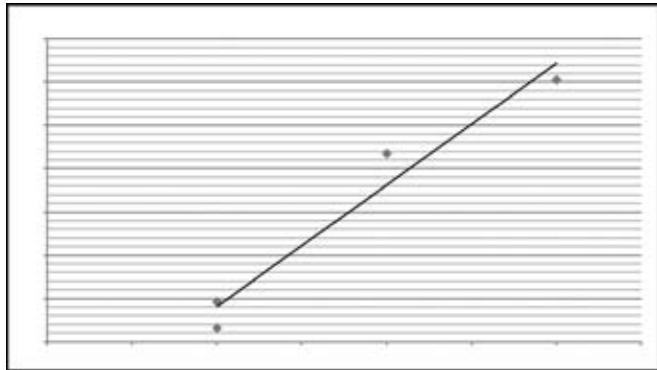


Figure 3: Motional resistance vs. etch hole diameter.

Results and Conclusion:

There was a definite trend when comparing etch hole diameter and signal strength. As etch hole size was decreased so did motional resistance (Figure 3), which indicates that a smaller etch hole produces a larger signal. We also discovered that the quality factor of our devices was independent of etch hole size. The actual drum diameter was independent of etch hole size as well.

Future Work:

Since the largest factor for motional resistance is oxide thickness, it is our greatest chance for increasing the signal. Therefore, going for an even smaller oxide thickness would increase the signal. Work could also be done to create an even smaller etch hole to see the results: a larger increase in signal power, no increase in signal power, or simply diminishing return in signal power. Lastly, multi-hole membranes should be studied to see how their geometries affect the electrical signal.

Acknowledgments:

I would like to thank the National Science Foundation and, in particular, the National Nanotechnology Infrastructure Network, for allowing me to be involved in this REU program, and the Intel Foundation for sponsoring my research. I would like to thank Harold Craighead for his support, and Darren Southworth and Josh Cross for their assistance. Acknowledgment is also given to the Cornell NanoScale Facility Staff, especially Melanie-Claire Mallison.